ELSEVIER

International Journal of Heat and Fluid Flow 19 (1998) 431–438

International Journal of HEAT AND FLUID FLOW

# Utilization of the Garteur swept wing data base for turbulence models evaluation in boundary layer calculations

M. Doussinault [a,*], C. Gleyzes [a], B. Aupoix [a], J.H.M. Gooden [b]

[a] *ONERA/MFE/DMAE, CERT, P.O. Box 4025, 31055 Toulouse Cedex, France*
[b] *NLR/NOP, P.O. Box 153, 8300 AD Emmeloord, The Netherlands*

**Abstract**

Three-dimensional flows are difficult test cases for turbulence models. Algebraic, two and five-equation models are tested here, in one or two-layer approaches, on the suction and the pressure side of the Garteur AD/AG07 swept wing. Direct and inverse mode computations are performed. Skin friction coefficient and shape factor distributions as well as turbulent kinetic energy profiles are shown at 68% of span where the flow is near separation at the suction side trailing edge, and accelerated in the last 30% of chord of the pressure side. Although providing fairly good skin friction predictions, the mixing-length model does not properly reproduce the mean velocity profiles for this type of three-dimensional flow. The two-layer approach (algebraic – five-equation) and the $k$-$\epsilon$ models are disappointing. Results of the $k$-$\varphi$ model are promising. The $k$-$\omega$ SST model, used in inverse mode, is the most efficient of the tested models, but has also some difficulties to predict with accuracy this type of flow. 

*Keywords:* Swept wing; Three-dimensional boundary layer; Turbulence; Turbulence models

## 1. Introduction

Experimental data concerning three-dimensional turbulent flows close to practical applications are rare. A Garteur action group led parallel experiments on this type of flow in the NLR/LST and ONERA/F2 wind tunnels. The model is a swept wing on which the pressure distribution in incompressible flow conditions is similar to the one of a supercritical transonic wing (Firmin and McDonald, 1988; Van den Berg, 1988; Gleyzes et al., 1993). Boundary layers are tripped very close to the attachment line on both sides of the model. The Reynolds number based on the mean chord $C$ is $3.3 \times 10^6$, and the incidence is 0.5°. For these experiments, two pressure probes (noted S2T in figures), and four hot-wire probes (noted S2F and S4F, respectively), as well as 3D-LDA were used to allow cross-checking. Results obtained in each wind tunnel by different experimental techniques are in good agreement and the similarity between the two flows is quite impressive. Thus, mean flow and turbulent characteristics of the AD/AG07 wing are regarded as reliable and accurate.

The suction side is characterized by a strong positive pressure gradient which leads to a nearly separated flow. The three-dimensional character of the flow is very important: wall deviation is about 50° at the trailing edge. On the pressure side, the flow is decelerated only between 30% and 70% of chord. Downstream, the acceleration induces a nearly collateral flow at the trailing edge. Despite these two different behaviors, the lag of the "shear stress vector" $(-\rho\overline{u'w'}, -\rho\overline{v'w'})$ behind the "mean strain rate vector" $((\partial U/\partial z), (\partial V/\partial z))$ can be observed on both sides of the wing.

Within the Garteur framework, this very detailed database is being used to evaluate the ability of classical turbulence models, initially developed for two-dimensional flows and extended to three-dimensional ones, to predict this type of steady 3D turbulent shear flow close to practical applications. The computation domain is limited from 20% to 95% in chord, and from 8% to 92% in span on the pressure and the suction sides. Each side is computed separately.

## 2. Reference frames and notations

As shown in Fig. 1, the reference Cartesian coordinate system is noted $(X_R, Y_R, Z_R)$. $X_R$ and $Z_R$ are in the plane of the tunnel wall on which the model is mounted, $Z_R$ being normal to the tunnel longitudinal axis. $Y_R$ is the rotation axis of the model. For a given constant span section, $C_S$ is the local chord and $X_S$ is the distance from the leading edge in the reference coordinate system, so that $X^1 = X_S/C_S$ is the dimensionless chord. The dimensionless span $X^2 = Y_R/S$ is also defined, where $S$ is the span of the wing. At last, $(X_B, Y_B, Z_B)$ is the local boundary layer coordinate system. $Z_B$ is the direction normal to the surface of the wing at the considered point. $X_B$ is tangent to the surface, pointing towards the trailing edge in the direction $X^2 = constant$. $Y_B$ completes this Cartesian system. $(U, V, W)$ and $(u', v', w')$ are the mean and fluctuating components of the velocity, the mean magnitude of which is noted $G$ and

* Corresponding author. E-mail: marc.doussinault@onecert.fr.

0142-727X/98/$ – see front matter 
PII: S0142-727X(98)10016-4

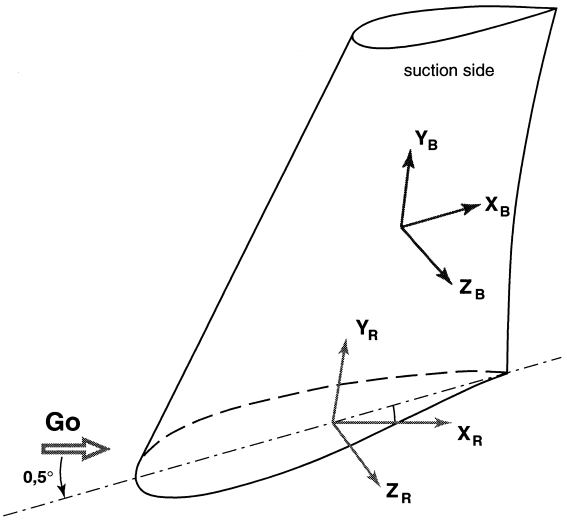


Fig. 1. Reference frame definitions.

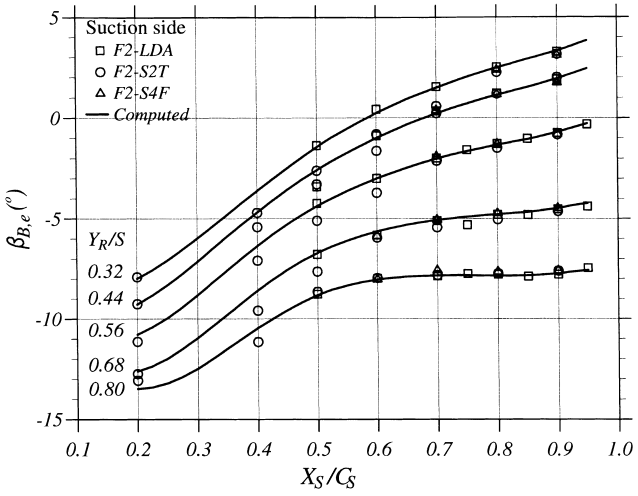


Fig. 2. Edge flow conditions: suction-side deviation.

deviation angle from $X^2 = constant$ lines is noted $\beta$. Subscripts e and w stand for edge flow and wall conditions, and the subscript 1 means that the velocity is expressed in the boundary layer frame in which the $X$ direction follows the local external streamwise direction.

## 3. Computational procedure

A three-dimensional boundary layer code, 3C3D, has been developed at ONERA since 1990 by Houdeville (1992) and Malecki (1994). The key feature of this code is to solve first order boundary layer equations in a local Cartesian system which allows not to compute Christoffel coefficients. Boundary layer equations are discretized following the local streamlines to take strictly into account the influence-dependence domains. It is possible to run computations in direct or inverse mode.

### 3.1. Boundary conditions

*Direct mode: Edge flow velocity.* In this case, edge flow conditions are the velocity magnitude ($G_e$) and direction ($\beta_{B,e}$). Unfortunately, measured edge flow velocity field is not available on the whole surface of the wing. Assuming that the normal pressure gradient is zero, the inviscid wall flow is computed using the experimental wall pressure coefficients (which have been measured in detail) and solving the Euler equations on the surface of the wing. This method gives good results on the suction side where the normal pressure gradient is actually negligible. Mean quadratic differences between computed edge flow angles and measured ones (0.1° for LDA, 0.5° for S2T) are lower than the accuracy of measurement techniques (Fig. 2). On pressure side, the relatively strong curvature of the wing induces a small normal pressure gradient which might explain why results are not as good as on the suction side (Fig. 3): there is up to 1° of difference between computed and experimental deviations. However, the boundary layer is thin enough to neglect the normal pressure gradient in boundary layer computations.

*Inverse mode: Displacement thicknesses.* Inverse mode is an interesting approach for nearly separated flows in boundary layer computations. For such three-dimensional cases, this method reduces the sensitivity of the models to the discretization scheme. Longitudinal $\delta_1$ and transverse $\delta_2$ displacement thicknesses deduced from experimental velocity profiles are imposed here as boundary conditions. These thicknesses are not known on a grid fine enough for computations. They are interpolated at the desired points. The first 10% after the starting up stations (from 20% to 30% of chord) are computed in direct mode, and then the computation is switched to inverse mode. There is no significant influence of the location of the switch to inverse mode on the suction side. However, it is important to begin inverse mode computation after 30% of chord on the pressure side, because inverse mode must not be initialized in the accelerated part of the computation domain from 20% to 30% of chord.

### 3.2. Lateral conditions

Boundary conditions have to be imposed at the borders of the computation domain (8% and 92% of span). Unfortunately, experimental data are not available in these span sections. Therefore, the conditions imposed on the lateral ends of the computation domain are those of a conical swept wing: it is assumed that the flow is invariant in the local spanwise direction, i.e. $\partial/\partial X^2 = 0$. Comparisons with experiments have to be done out of the domain of influence of these lateral conditions. From external and wall streamlines, the domain of validity

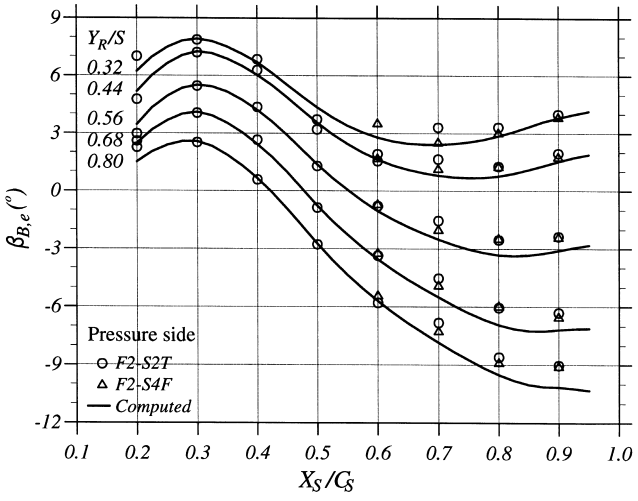


Fig. 3. Edge flow conditions: pressure-side deviation.

of the computation at the trailing edge is shown to be reduced and extends from 38% to 74% of span on the suction side and from 26% to 80% on the pressure side.

### 3.3. Initial conditions

To start boundary layer computations, initial velocity profiles are imposed at 20% of chord. Experimental profiles can not be used directly (because of scatter and lack of measurement points near the wall). Longitudinal profiles are built from the shape factor $H$ and the integral thickness $\theta_{11}$ using the Galbraith and Head analytical expressions. Starting from estimated $H$ and $\theta_{11}$ deduced from experimental velocity profiles, $H$ and $\theta_{11}$ are optimized in an iterative process to minimize the quadratic error between computed and experimental profiles (Fig. 4, dimensionless longitudinal velocity $U_1/G_e$ function of dimensionless distance normal to the wall $Z_B/C$). Transverse profiles are built using the integral thickness $\theta_{21}$ and the cross-flow angle at the wall $\beta_0$, and assuming they are triangular in the hodograph plane. This assumption is not always verified on the suction side, but cross-flow magnitude is weak compared to edge velocity magnitude (lower than 2%) and does not significantly influence computations downstream.

## 4. Turbulence models

Only a short selection of the turbulence models tested on this flow are presented here. A detailed description of the theorical and numerical approaches can be found in Doussinault (1998).

### 4.1. Algebraic model

The Garteur action group decided that a simple turbulence model should be used by all the participants to facilitate computation comparisons. The chosen model is an algebraic eddy viscosity model derived from the Cebeci–Smith mixing length model (noted LMS) (Cebeci and Smith, 1974). It is a two-layer model. In the inner layer a mixing-length formulation is used with the Van Driest damping function to express the eddy viscosity $\nu_{t_i}$:

$$\nu_{t_i} = \left[\chi z \left(1 - e^{-z^+/26}\right)\right]^2 \sqrt{\left(\frac{\partial U}{\partial z}\right)^2 + \left(\frac{\partial V}{\partial z}\right)^2},$$

where $\chi = 0.41$ and $z^+$ is the normal distance from the surface in wall units. In the outer region, the eddy viscosity $\nu_{t_0}$ is expressed as a function of the external velocity $G_e$, the longitudinal displacement thickness $\delta_1$ and the Klebanoff intermittency function

$$\nu_{t_e} = \alpha G_e \delta_1 \left(1 + 5.5\left(\frac{z}{\delta}\right)^6\right)^{-1}$$

with $\alpha = 0.0168$ and $\delta$ being the 0.998% boundary layer thickness. No junction point is needed as the final expression for the eddy viscosity is

$$\nu_t = \nu_{t_0} \tanh\left(\frac{\nu_{t_i}}{\nu_{t_0}}\right).$$

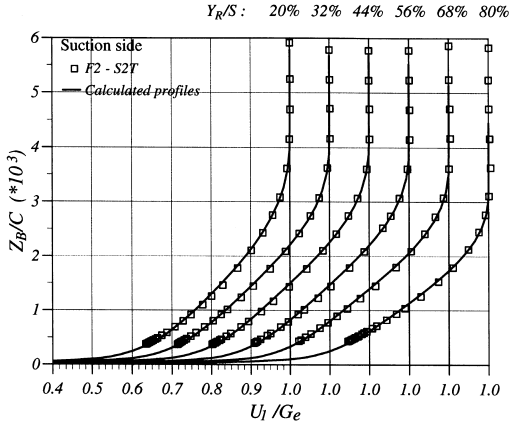


Fig. 4. Initial longitudinal velocity profiles. Suction-side.

### 4.2. Two-equations k-ϵ model

The So–Zhang–Speziale model (noted $k$-$\epsilon$ SZS in figures) will be the only $k$-$\epsilon$ model presented here (So et al., 1991). In the case of the Garteur AD/AG07 wing, this model gives slightly better results than the other $k$-$\epsilon$ models implemented in 3C3D code.

### 4.3. Two-equation k-ω SST

Initially developed by Wilcox (1988), $k$-$\omega$ models are the second well known family of two-equation models. The equation for the dissipation $\epsilon$ is replaced by an equation for the specific dissipation rate $\omega = \epsilon/(C_\mu k)$ with $C_\mu = 0.090$. The advantage of this model is that there is no damping function near the wall and that it performs better in positive pressure gradient conditions than $k$-$\epsilon$ models.

However, Menter (1994) showed that the results of this model depend on the free-stream values of the specific dissipation imposed outside the boundary layer. To remove the dependency of the $k$-$\omega$ model to the edge condition, Menter (1994) first proposed to include the cross-diffusion term $((\partial k/\partial z)(\partial\omega/\partial z))$. Then, using appropriate blending functions, this model behaves like a $k$-$\omega$ model near the wall and like a $k$-$\epsilon$ model in the outer part of the boundary layer.

For positive pressure gradient flows, the production of $k$ exceeds its dissipation in a large part of the boundary layer. This generally leads to an over-prediction of the turbulent shear stress. On the other hand, the Bradshaw's assumption tells that the turbulence structural parameter $a_1$ is nearly constant through the boundary layer:

$$2a_1 = \frac{\sqrt{\overline{u'w'}^2 + \overline{v'w'}^2}}{k} \sim 0.31 .$$

Menter (1994) invokes this assumption in the SST model (noted $k$-$\omega$ SST) to use an eddy viscosity formulation that guarantees that the shear stress is not higher than $2a_1\rho k$.

### 4.4. Two-layer: k-ω/k-φ model

Cousteix et al. (1997) developed a new model which has the same numerical stability and good predictions ability as the $k$-$\omega$ model but which is not sensitive to free-stream values. They obtain a $k$-$\varphi$ model with $\varphi = \varepsilon/\sqrt{k}$. The tests have shown that the model produces good results for free shear flows and for the outer region of boundary layers with positive pressure gradient. Wall damping functions are needed to reproduce correctly the buffer region. At the present stage of the development of the model, these functions are not fixed yet. However, the $k$-$\varphi$ model can be used in the outer part of the boundary layer using a two-layer approach. The standard $k$-$\omega$ model is then used in the near wall region. The $k$-$\omega$ model is switched to the $k$-$\varphi$ model at the end of the logarithmic region. The dependency of the model on the location of the

switching point has been studied. Results of the model are not changed if the location of the switching point is imposed 25% higher or lower than the end of the logarithmic region.

### 4.5. Two-layer: Algebraic – five-equation model

This model (noted LMS/IP-GL) is also a two-layer model. The LMS model is used in the inner part of the boundary layer. In the outer region, transport equations for the Reynolds stresses are solved. For the redistribution term, the Rotta formulation is used for the non-linear part and the isotropization of production model (IP) proposed by Naot et al. (1973) is used for the rapid part. The Gibson–Launder damping functions (GL) are included in the model to account for wall boundary effects (Gibson and Launder, 1978). Five equations are solved (in addition to the momentum and continuity equations): for the turbulent kinetic energy $k$, for the dissipation $\epsilon$, for the longitudinal and transverse Reynolds stresses $\overline{u'w'}$ and $\overline{v'w'}$ and for the normal Reynolds stress $\overline{w'^2}$. With the thin layer approximation and the IP model, only these three Reynolds stresses are needed for computation. Equations of this model will not be detailed in this paper. For further informations, see Malecki et al. (1993) for example. One must keep in mind that this simple Reynolds stress model is not able to produce any lag of the shear stress vector behind the mean velocity gradient vector. The point where the turbulence model is switched from LMS to IP-GL is fixed at $z_B^+ = 60$ in wall units, just after the beginning of the logarithmic region. By locating this point at $\pm 25\%$ from its initial value, the friction coefficient is changed by $\mp 5\%$. Although this dependency is important, it is of the order of magnitude of the accuracy of the experimental skin friction coefficient.

## 5. Results and discussion

The normal grid dependency of the models has been studied. It has been found that, with more than 150 points in the normal direction, the models were no more sensitive to the grid. In the computations, it is imposed that the distance from the wall of the first two or three grid points is smaller than one in wall units.

### 5.1. General trends

Some examples of results concerning skin friction and shape factor at 68% of span in direct and inverse mode are given in Figs. 5 and 6 for suction and pressure side respectively. The experimental skin friction is estimated assuming that the velocity profiles satisfy the logarithmic law. At some stations,

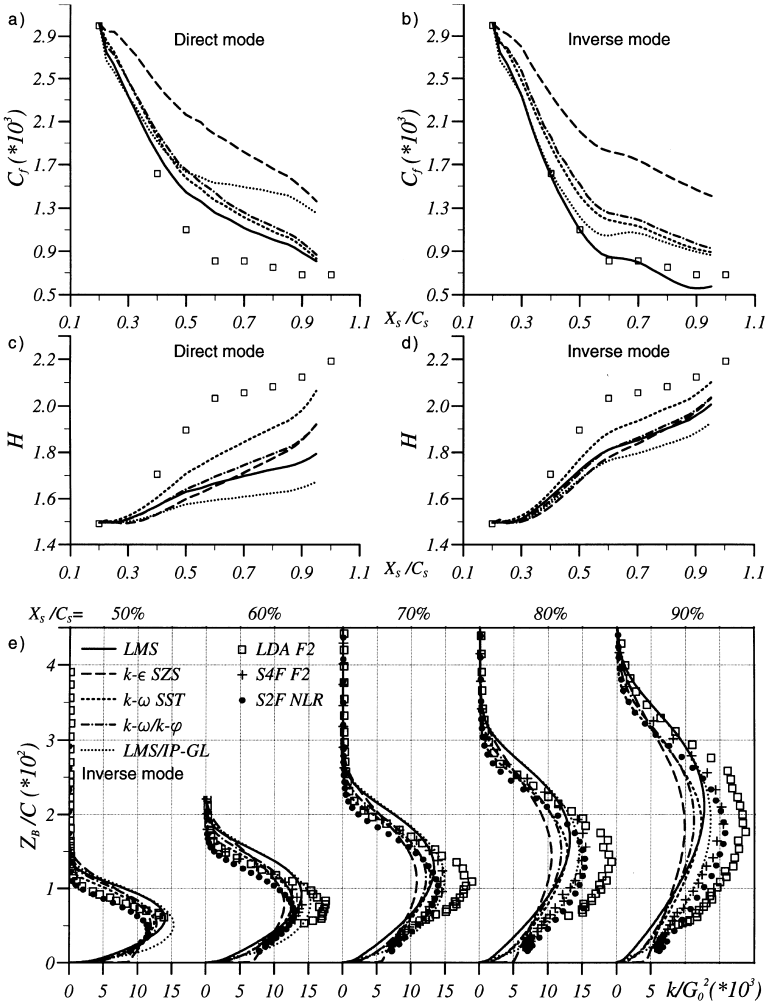


Fig. 5. Suction-side. Comparison of different turbulence models with experiment at 68% of span. Friction coefficient: (a) direct mode; (b) inverse mode. Shape factor: (c) direct mode; (d) inverse mode. (e) Kinetic turbulent energy profiles from 50% to 90% of chord in inverse mode.

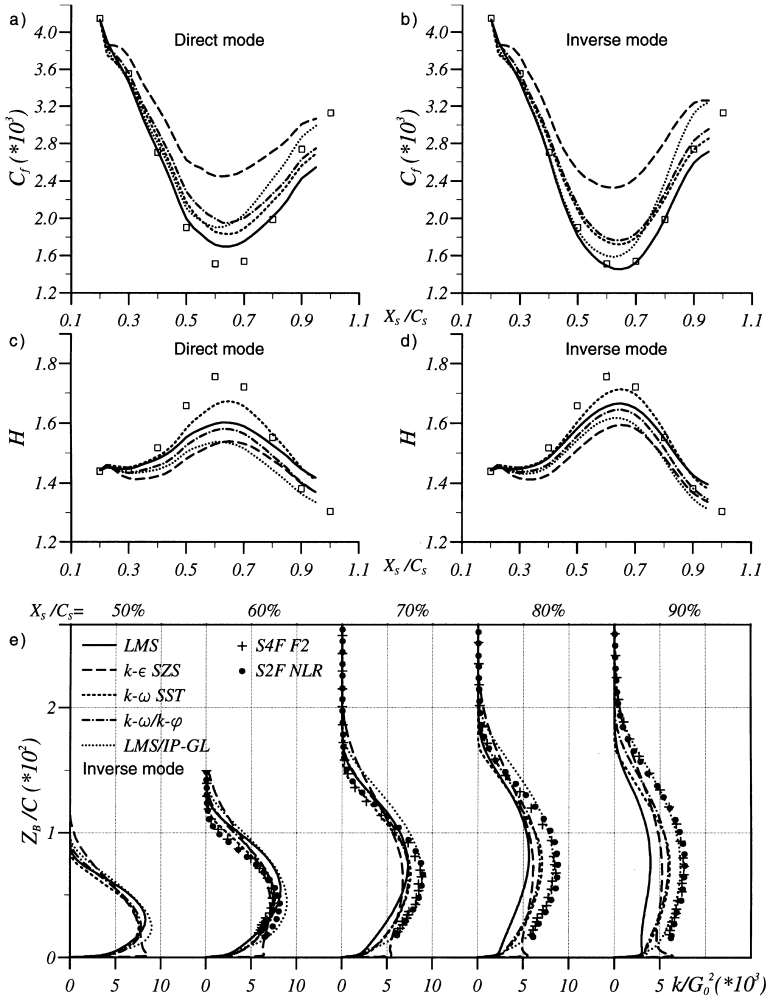


Fig. 6. Pressure-side. Comparison of different turbulence models with experiment at 68% of span. Friction coefficient: (a) direct mode; (b) inverse mode. Shape factor: (c) direct mode; (d) inverse mode. (e) Kinetic turbulent energy profiles from 50% to 90% of chord in inverse mode.

this skin friction coefficient was compared to skin friction gauges measurements: a relatively good agreement was obtained.

In direct mode, the skin friction is over-estimated and models are not able to reproduce the plateau between 60% and 100% of chord on the suction side nor to reach the minimum of $C_f$ at 60% of chord on the pressure side. In inverse mode, models yield a better skin friction prediction even if the level remains higher than in the experiment. Models underrate the shape factor, even in inverse mode. The wall shear stress deviation (not shown here) is also underestimated in direct mode, but is quite well estimated in inverse mode by SST model. Improvements gained in inverse mode are less important on the pressure side where the decelerated part of the flow in less important than on the suction side.

Concerning turbulence, dimensionless kinetic energy $k/G_0^2$ profiles obtained in inverse mode are presented in Figs. 5(e) and 6(e). Some discrepancies are seen between LDA and hot-wire measurements. Interference between the probe-support and the model, combined with a high local turbulence level may explain these differences. Gooden et al. (1997) showed that hot-wire technique tends to underestimate turbulence levels whereas laser anemometry slightly overestimates them.

In direct mode (not shown here) as well as in inverse mode, turbulent quantities are quite well estimated up to 60% of chord, with a maximum of the turbulent kinetic energy far from the wall characteristic of adverse pressure gradient flows. Downstream 60% of chord on the pressure side, models still predict the good shape of the turbulent profiles, but the level of the maximum decreases to reach an underestimation of 40% on $k$ at 90% of chord on the suction side. Models behave similarly on the pressure side, but, excepted for the LMS/IP-GL model, the decrease of the maximum of $k$ is more important because the pressure gradient is negative near the trailing edge. Results obtained on $\overline{u'w'}$ in direct or inverse mode do not differ much with the models (excepted at 80% and 90% of chord on the pressure side) and are 20–30% lower than LDA measurements. On the suction side, inverse mode has an important effect, particularly on LMS and LMS/IP-GL models, and increases the level of turbulent quantities, which are, however, still lower than experimental ones. The effect of inverse mode on turbulent quantities is less important on the pressure side. On both sides, in inverse mode, the turbulent layer thickness is overestimated on a large part of the computation domain excepted from 80% of chord to the trailing edge.

### 5.2. LMS model

On both sides, the algebraic model (solid lines in figures) yields the best prediction of the skin friction coefficient in direct and inverse mode (Figs. 5(a), 5(b), 6(a) and 6(b)). Unfortunately, the shape factor (Fig. 5(c) and (d)) and the de-

viation are largely underestimated on the suction side. Even if inverse mode seems to give better results it is because the external velocity magnitude is underestimated by nearly 10% at 90% of chord (Fig. 7) and induces a more decelerated flow than in the experiment. On the pressure side, shape factor computations are closer to the experiment, particularly in inverse mode (Fig. 6(c) and (d)). On the suction side, as all the other models, the turbulent kinetic energy is underestimated (for this model, the kinetic energy is estimated using the turbulence structural parameter, which in supposed to be constant: $a_1 = 0.15$). Near the pressure side trailing edge, the acceleration induces a fall in the turbulent quantities much more important than reported by the experiment (Fig. 6(e)).

As mixing length models are equilibrium models they are able to reproduce the near wall behavior (good $C_f$ prediction) but not the shape of the velocity profile in the outer region (poor $H$ prediction). This behavior may be due to an overestimation of the slope of the velocity profiles in the logarithmic region, as shown in the analysis of Huang and Bradshaw (1995) for two-dimensional flows in positive pressure gradient conditions. In addition, it is important to moderate the good results obtained in inverse mode because external conditions are then not well predicted on the suction side as well as on the pressure side.

### 5.3. $k$-$\epsilon$ SZS model

The $k$-$\epsilon$ model (long dash lines in figures) gives, for this flow, quite poor results. The skin friction coefficient is largely overestimated, even in inverse mode (Figs. 5(a), 5(b), 6(a) and 6(b)). This induces a large increase of $k$ near the wall (Figs. 5(e) and 6(e)). On the suction side, the evolution of $H$ exhibits a nearly constant slope from 40% to 90% of chord in direct and inverse mode whereas there is an experimental break at 60% of chord (Fig. 5(c) and (d)). On the pressure side, the flow is decelerated only from 30% to 70% of chord and the pressure gradient is less important than on the suction side. However the $k$-$\varepsilon$ model is not able to reproduce the fall of the skin friction coefficient up to 60% of chord (Fig. 6(c) and (d)).

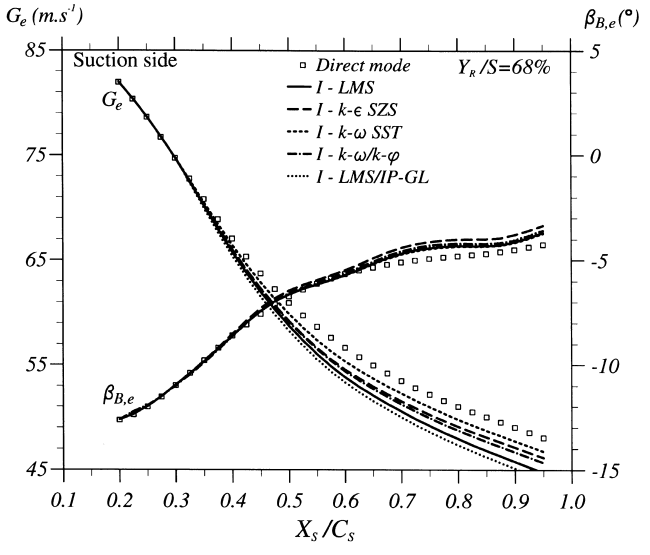


Fig. 7. Chord-wise evolution of edge flow velocity (magnitude and direction) computed in inverse mode. Comparison with direct mode imposed values. 68% of span, suction-side.

The difficulties of $k$-$\epsilon$ models in positive pressure-gradient conditions are well illustrated here. For this flow far from equilibrium where production exceeds dissipation in a large part of the boundary layer, it has been shown that the SZS $k$-$\varepsilon$ model overpredicts the structure parameter (overprediction of the turbulent shear-stress compared to the level of the turbulent kinetic energy). This may partly explain the poor results obtained with this model.

### 5.4. $k$-$\omega$ SST model

In direct mode on the suction side, $k$-$\omega$ model (short dash lines in figures) give the same $C_f$ evolution as LMS model (Fig. 5(a)) but yields much better shape factor prediction (Fig. 5(c)). In inverse mode, external velocity conditions are quite well predicted (less than 2% of difference between direct and inverse mode edge flow velocity (Fig. 7)). Inverse mode also improves computations for the friction coefficient and the shape factor (Figs. 5(b) and 5(d)). The maximum difference between experimental and computed shape factor decreases from 20% in direct mode to 8% in inverse mode. For turbulent kinetic energy (Fig. 5(e)), computations results are still more than 30% lower than LDA measurements (for the maximum value of $k$ in the boundary layer at 90% of chord). But, contrary to other models, the boundary layer thickness is not overestimated.

On the pressure side (Fig. 6), the SST model yields good results in direct mode, particularly for the shape factor (Fig. 6(a) and (c)). Inverse mode improves moderately the results on SST model (Fig. 6(b) and (d)) and the edge flow velocity is within 2% of the direct mode one. As the flow is accelerated (70–90% of chord) the kinetic energy becomes underestimated, as well as the boundary layer thickness which even decreases between 80% and 90% whereas it goes on increasing (moderately) experimentally (Fig. 6(e)).

Two main reasons are likely to explain why this model yields better results than the other tested models. First, $k$-$\omega$ models show the ability to reproduce quite well the logarithmic law, even in positive pressure gradient conditions (Huang and Bradshaw, 1995). Secondly, the formulation of the eddy viscosity in the SST model prevents the structure parameter to exceed the two-dimensional value of 0.15 (Menter, 1994).

### 5.5. $k$-$\omega$/$k$-$\varphi$ model

Results of the $k$-$\omega$/$k$-$\varphi$ model (dot-dash lines in figures) are close to SST model ones. This is particularly visible on the skin friction coefficient for both modes and sides (Fig. 5(a) and (b) and Fig. 6(a) and (b)). Differences are more important on the shape factor. In inverse mode on the suction side (Fig. 7) the external flow direction is well predicted but the magnitude of the external velocity is under-estimated by 5% at 90% of chord. $k$-$\omega$/$k$-$\varphi$ and SST models show similar turbulent kinetic energy profiles. On the suction side (Fig. 5(e)), the $k$-$\omega$/$k$-$\varphi$ model predicts a maximum of $k$ a bit lower than the SST model. Another difference between these models is that the $k$-$\omega$/$k$-$\varphi$ model yields a slightly thicker boundary layer. In particular on the pressure side (Fig. 6(e)), the boundary layer thickness does not decrease in the accelerated region.

In the outer region, the $k$-$\varphi$ model seems to be a good alternative to $k$-$\varepsilon$ models (poor predictions for decelerated flows) and to the original $k$-$\omega$ model (sensitive to external values). This model needs now to be refined in the vicinity of the wall.

### 5.6. LMS/IP-GL model

The two-layer approach with five equations in the outer part of the boundary layer (dot lines in figures) is somewhat

disappointing. It gives reasonably good results for turbulent quantities especially in inverse mode (Figs. 5(e) and 6(e)). The general shape of the evolutions of $C_f$ and $H$ is quite well reproduced: in direct mode on the suction side, it is the only model to present a significative break in the slope of the skin friction evolution at 50% of chord. But this break seems to occur too early and the levels of the skin friction and the shape factor are not the good ones. Inverse mode improves computations as it is particularly visible on skin friction coefficient predictions (Figs. 5(b) and 6(b)), but the computed shape factor is still 15% lower than the experimental one (Figs. 4 and 5(d)). As for the LMS model, the boundary layer edge conditions are not well predicted in inverse mode.

Even though LMS and LMS/IP-GL have the same turbulence model near the wall, these models do not give the same $C_f$ evolutions. Outer region turbulence model plays an important part in wall shear stress predictions.

### 5.7. Anisotropy of viscosity

Experimentally, the lag of the shear stress vector behind the mean velocity gradient vector is about 10° on both sides of the wing. This anisotropy is not taken into account with eddy viscosity models and this could explain the difficulties of the models to predict this three-dimensional flow. An anisotropic eddy viscosity was introduced in some models following the formulation of Rotta (1967, 1977)

$$-\overline{u'w'} = \nu_t\left(a_{xx}\frac{\partial U}{\partial z} + a_{xy}\frac{\partial V}{\partial z}\right), \quad -\overline{v'w'} = \nu_t\left(a_{xy}\frac{\partial U}{\partial z} + a_{yy}\frac{\partial V}{\partial Z}\right)$$

with

$$a_{xx} = \frac{U^2 + TV^2}{U^2 + V^2}, \quad a_{yy} = \frac{TU^2 + V^2}{U^2 + V^2}, \quad a_{xy} = (1 - T)\frac{UV}{U^2 + V^2}.$$

The value of the anisotropy factor $T$ is taken lower than 1 to create artificial anisotropy. This formulation is not Galilean-invariant but is a good first approach for anisotropy modeling. In the Garteur experiment the anisotropy factor is about 0.8 in a large part of the studied domain.

For all the tested models (mixing length, $k$-$\varepsilon$ and $k$-$\omega$), the effect of $T$ factor is important on the wall shear stress direction but is scarcely visible on the skin friction coefficient and the shape factor, even for weak values of $T$ such as 0.5. Turbulent quantities are not significantly affected by the anisotropy factor, excepted the transverse Reynolds stress $\overline{v'w'}$ which is increased moderately.

From these results it seems that the modeling of the anisotropy of viscosity is not the key point for this flow: the main problem is the difficulty of the models to react to the longitudinal pressure gradient.

## 6. Conclusion

This study points out that most of the turbulence models tested are not able to foresee with accuracy this type of practical turbulent shear flow.

- On the suction side, the flow is continuously decelerated and is nearly separated at the trailing edge. The three-dimensional character of the flow is important and the turbulent shear stress direction lags of about 10° behind mean strain rate one. It seems that turbulence modeling difficulties are principally due to the strong positive pressure gradient, and only to a lower degree, to the anisotropy of eddy viscosity. Inverse mode computation is a good way to improve the results for such decelerated flows, but it must be checked that the external velocity conditions are well reproduced.
- On the pressure side, the pressure gradient is positive from 30% to 70% of chord and the flow is accelerated in the rear load region. Models perform better than on the suction side but skin friction coefficient remains overestimated and the shape factor underestimated. Inverse mode improves the results but has a smaller effect than on the suction side because the adverse pressure gradient is less important.

Taken as a whole, $k$-$\omega$ SST model in inverse mode is the best of the tested models, whereas $k$-$\epsilon$ model gives poor results. This classification is the same as the one obtained in former studies for two-dimensional flows in positive pressure gradients.

For the future, full Reynolds Stress Models will be tested on this difficult three-dimensional test case. It will be also interesting to study the behavior of the models in the highly asymmetrical wake of the wing.

## Acknowledgements

Financial support of the ONERA contribution was provided by the French government agency SPAé.

## References

Cebeci, T., Smith, A.M.O., 1974. Analysis of turbulent boundary layers. In: Applied Mathematics and Mechanics, vol. 15. Academic Press, New York.

Cousteix, J., Saint-Martin, V., Messing, R., Bézard, H., Aupoix, B., 1997. Development of the $k$-$\varphi$ turbulence model. In: Proceedings of the 11th Symposium on Turbulent Shear Flows. Grenoble, France.

Doussinault, M., 1998. Étude de modèles de turbulence appliqués à l'écoulement autour de l'aile GARTEUR AD/AG07 (couche limite et sillage) Ph.D. Thesis, ENSAE, Toulouse.

Firmin, M.C.P., McDonald, M.A., 1988. The design of the Garteur low aspect-ratio wing for the use in validation of shear layer and overall flow prediction methods. In: FDP Symposium on Validation of Computational Fluid Dynamics. AGARD CP 437 (GARTEUR AD(AG07) TP032) Lisbonne, 2–5 May.

Gibson, M.M., Launder, B.E., 1978. Ground effects on pressure fluctuation in the atmospheric boundary layer. J. Fluid Mech. 86 (3), 491–511.

Gleyzes, C., Maciel, Y., Cousteix, J., Gooden, J.H.M., Reinders, W., van den Berg, B., 1993. Three-dimensional turbulent flow around the GARTEUR swept wing, Selected features. In: Proceedings of the Ninth Symposium on Turbulent Shear Flows. Kyoto, Japan.

Gooden, J.H.M., Gleyzes, C., Maciel, Y., 1997. Experimental study of the flow around two scaled 3D swept wings. AIAA Paper 97-2020, 28th Fluid Dynamics Conference, Snowmass, Col.

Houdeville, R., 1992. Three-dimensional boundary layer calculation by a characteristic method. In: Proceedings of the Fifth Symposium of Numerical and Physical Aspects of Aerodynamic Flows, Long Beach.

Huang, P.G., Bradshaw, P., 1995. Law of the wall for turbulent flows in pressure gradients. AIAA Journal 33 (4), 624–632.

Malecki, P., 1994. Étude de modèles de turbulence pour les couches limites tridimensionnelles. Ph.D. Thesis, ENSAE, Toulouse.

Malecki, P., Cousteix, J., Houdeville, R., 1993. Three-dimensional boundary layer calculations with two-layer turbulence models. Fifth IAHR International Symposium on Refined Flow Modelling and Turbulence Measurements. Ed. ENPC, Paris, 7–10 September.

Menter, F.R., 1994. Two-equation eddy-viscosity turbulence models for engineering applications. AIAA Journal 32 (8), 1598–1605.

Noat, D., Shavit, A., Wolfshtein, M., 1973. Two-point correlation model and the redistribution of Reynolds stresses. The Physics of Fluids 16 (6), 738–743.

Rotta, J.C., 1967. Turbulent boundary layers in compressible flow. In: Progress in Aeronautical Sciences. Pergamon Press, Oxford.

Rotta, J.C., 1977. A family of turbulence models for three-dimensional thin shear layer. In: Proceedings of the First Symposium on Turbulent Shear Flows. University Park, Pennsylvania.

So, R.M.C., Zhang, H.S., Speziale, C.G., 1991. Near wall modeling of the dissipation rate equation. AIAA Journal 29 (12), 2069–2076.

Van den Berg, B., 1988. A European collaborative investigation of the three-dimensional turbulent shear layers of a swept wing. AGARD-CP-438.

Wilcox, D.C., 1988. Reassessment of the scale-determining equation for advanced turbulence models. AIAA Journal 26 (11), 1299–1310.